Lawrence Berkeley National Laboratory
Recent Work

Title
Unsaturated Ligands Seed an Order to Disorder Transition in Mixed Ligand Shells of CdSe/CdS Quantum Dots.

Authors
Balan, Arunima D
Olshansky, Jacob H
Horowitz, Yonatan
et al.

Peer reviewed

Unsaturated Ligands Seed an Order to Disorder Transition in Mixed Ligand Shells of CdSe/CdS Quantum Dots

Arunima D. Balan,[†⊥§] Jacob H. Olshansky,[†⊥§] Yonatan Horowitz,[†⊥ §‡] Hui-Ling Han,[†⊥§] Erin A. O'Brien,[†⊥§] Lucio Tang,[†] Gabor A. Somorjai,[†⊥§] and A. Paul Alivisatos[†⊥§#*]

†Department of Chemistry and #Department of Materials Science and Engineering, University of California, Berkeley, Berkeley, California 94720, United States

⊥Material Sciences Division, Lawrence Berkeley National Laboratory, Berkeley, California 94720, United States

§ Kavli Energy NanoScience Institute, Berkeley, California 94720, United States

Abstract:

A phase transition within the ligand shell of core/shell quantum dots is studied in the prototypical system of colloidal CdSe/CdS quantum dots with a ligand shell composed of bound oleate (OA) and octadecylphosphonate (ODPA). The ligand shell composition is tuned using a ligand exchange procedure and quantified through proton NMR spectroscopy. Temperature-dependent photoluminescence spectroscopy reveals a signature of a phase transition within the organic ligand shell. Surprisingly, the ligand order to disorder phase transition triggers an abrupt *increase* in the photoluminescence quantum yield (PLQY) and full-width at half maximum (FWHM) with increasing temperature. The temperature and width of the phase transition shows a clear dependence on ligand shell composition, such that QDs with higher ODPA fractions have sharper phase transitions that occur at higher temperatures. In order to gain a molecular understanding of the changes in ligand ordering, fourier-transform infrared and vibrational sum frequency generation spectroscopies are performed. These measurements confirm that an order/disorder transition in the ligand shell tracks with the photoluminescence changes that accompany the order disorder ligand phase transition. The phase transition is simulated through a lattice model that suggests that the ligand shell is well-mixed, and does not

have completely segregated domains of OA and ODPA. Furthermore, we show that the unsaturated chains of OA seed disorder within the ligand shell.

The tunable ligand shell of colloidal quantum dots (QDs) provides a convenient post-synthetic handle to modulate nanoparticle properties, including solubility,[1-3] coupling with other nanocrystals,[3-5] and photoluminescence quantum yield (PLQY).[3,6,7] Standard hydrophobic QDs are capped with ligands that have long (C10+) organic tail groups and a variety of binding groups including amines, phosphines, carboxylic acids, and phosphonic acids.[8] The interactions between and within the aliphatic chains can lead to a variety of conformations within the ligand shell. In these systems, there is an enthalpic force for chains to pack, while there is an entropic force driving disorder in the chains. This can result in a temperature-driven phase transition from an ordered, low-temperature, phase to a disordered high-temperature phase. Such phase transitions have been previously observed in amine and thiolate capped cadmium selenide (CdSe) QDs,[9,10] and have been studied computationally on cadmium sulfide (CdS) QDs and nanorods.[11,12] A similar transition has also been studied in alkanethiolate-capped Au nanoparticles.[13-15] The phase transitions within the ligand shell of QDs have analogous features to transitions studied in other important systems that have significant aliphatic chain interactions, including self-assembled monolayers[16] and phospholipid bilayers.[17,18] Due to their solution-processability and finite size, QDs offer a convenient model system to better understand these aliphatic chain phase transitions more generally.

Furthermore, understanding the specifics of ligand phase transitions on QD surfaces is of interest since ligand conformation can affect a wide range of QD properties. Molecular dynamics simulations have shown that the order/disorder phase transition in the ligand shell of CdS nanorods modulates the interaction potential between rods, resulting in a nanorod attraction in the ordered phase.[11] Order-disorder changes in ligand configuration on the QD surface can also affect their solubility.[19,20] Similar arguments apply to QD superlattice studies, where the structure of the ligand shell can determine the structure of the superlattice.[21] For example, the distance between PbS QDs in a superlattice does not depend linearly on the number of carbons in the aliphatic chains. Shorter chains accommodate extended ligands while longer ligands can adopt a more disordered, and hence compact, profile.[22,23] Finally, the conformation of the ligand shell can strongly impact the shell permeability, which is relevant in a number of applications.[24] For example,

the Au deposition motif on CdS nanorods changes from depositing on the tips to depositing on the sides as both the composition of the ligand shell and temperature change, which corresponds to a phase transition in the ligands.[10,25]

It was somewhat more surprising when reports first appeared that the photoluminescence of core-shell quantum dots is influenced, not just by the type and number of organic ligands on the surface, but also by subtle changes in their ordering.[10,26,27] When the ligand shell undergoes an order/disorder phase transition the PLQY of the system increases, as observed in CdSe QDs capped with amines,[10] water-soluble CdTe QDs,[26] and in CdSe/ZnS core-shell QDs.[27] This increase in PLQY, or decrease in total nonradiative rate, is likely due to a decrease in surface trapping when the ligands disorder. The precise nature of this trap state is unknown, but the presence of such a trap for the ordered low temperature configuration is consistent with the strong influence surface ligands can have on QD PLQY. For example, changes in surface dipole moment have been shown to shift the band edge positions of QDs.[28,29] Furthermore, small changes in ligand coverage and passivation can have significant impacts on QD charge trapping behaviors.[3,8] For the purposes of observing the phase transition in the ligand shell, the presence of this trap is useful, as the change in PLQY can provide a sensitive handle on the ligand conformation. Furthermore, understanding how disordered and ordered states of ligand shells influence the coupling between core and surface energy levels of quantum dots will aid in the deliberate design strategies of ligand shells that can order in a way that produces desirable QD properties. In the work presented here, we explore how the composition of a saturated/unsaturated mixed ligand shell can control an order-disorder phase transition.
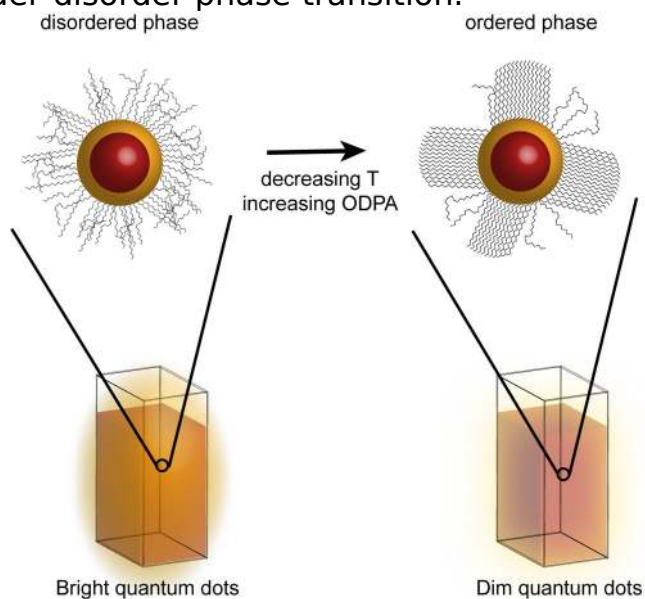
Figure 1: Schematic of a ligand order/disorder transition in nanoparticle systems and the associated change in QD photoluminescence

Although significant work has been performed on nanoparticle systems with single-component ligand shells, precise studies of mixed-ligand shells are more limited, likely due to the difficulty of quantifying mixed-ligand shell compositions. In this work, we choose to study how the ligand composition impacts the structure in mixed ligand shells of octadecylphosphonic acid (HODPA), bound as singly-deprotonated octadecylphosphonate (ODPA) and oleic acid (HOA), bound as oleate (OA), on CdSe/CdS QDs. We observe a phase transition *via* temperature-dependent photoluminescence (PL) spectroscopy, shown schematically in Figure 1. In order to better understand the molecular nature of the phase transition, we then perform variable-temperature Fourier transfer infrared (VT-FTIR) and sum frequency generation (SFG) vibrational spectroscopies, and show that the phase transition involves a disordering of the ligand shell. The combination of temperature-dependent PL and IR spectroscopies yields powerful insights that allows for correlation between structural and optical properties. We also model the presence of OA in the ligand shell using a modified lattice model, which is used to gain information about the microscopic structure of the phase transition.

Results/Discussion:
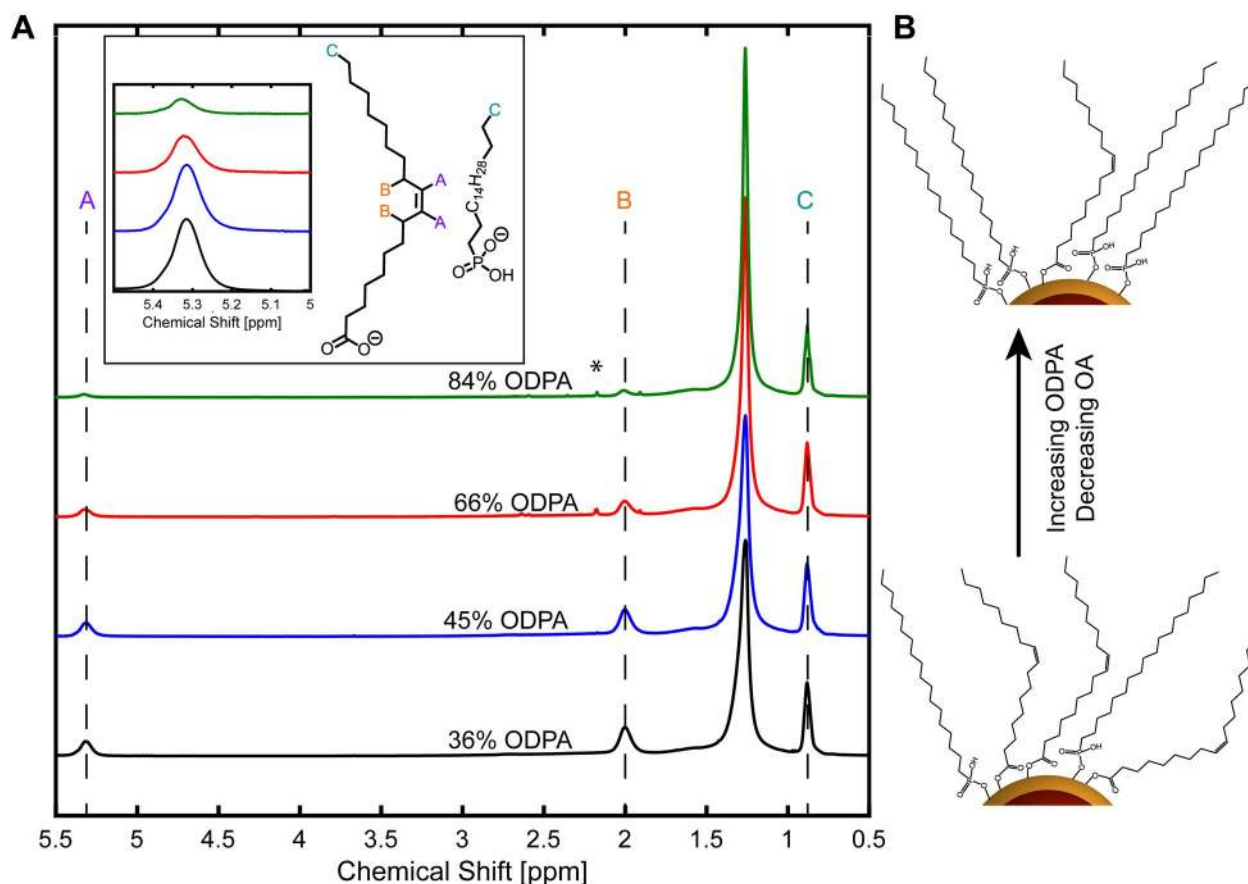
Figure 2: A) quantitative proton NMR spectra of all QD samples. The inset highlights the decrease in the vinyl peak as more ODPA is exchanged into the ligand shell and shows the structure and relevant protons of the ligands used. The asterisk indicates a small acetone impurity. B) Schematic of the ligand exchange process, displaying a small fraction of the QD surface and the bound ligands.

CdSe/CdS QDs are a prototypical II-VI material, and their ease of synthesis and high PLQY allow us to perform many temperature-dependent optical measurements. In addition, it is possible to synthesize thin-shell QDs with high PLQY, which is necessary for the QD PL to be sensitive to the surface. Furthermore, we can control the ligand structure on the surface of QDs by introducing only known precursor ligands during the synthesis. The core CdSe QDs were synthesized (following Carbone *et al.*) in trioctylphosphine oxide (TOPO), trioctylphosphine (TOP) and HODPA.[30] After purification, these QDs are bound exclusively with ODPA ligands (no TOP is bound).[31] The CdS shell growth is performed using a modified literature procedure, *via* slow addition of cadmium oleate and octanethiol in 1-octadecene.[32] The only alteration from the previously reported shelling reaction is in the removal of oleylamine as a solvent.[33] This is to enable accurate NMR quantification, since the vinyl proton signatures (~5-5.5 ppm) in oleylamine and OA overlap.

5

Additionally, avoiding amines is desirable since in high concentrations they are known to strip surface Cd and can further change the structure of the ligand shell.[8] The CdSe/CdS synthesis procedure as-performed results in a ligand shell composed only of OA and ODPA, which allows for subsequent NMR quantification. For the thin-shell CdSe/CdS studied in this work, the change in shelling procedure had no significant impact on the QD shape, as shown in the TEM of the as-synthesized QDs (see Supporting Information).

Ligand exchange and quantification

Ligand exchanges on the native sample were conducted in THF (due to limited HODPA solubility in other solvents), by adding a sub-stoichiometric amount of HODPA. We assume a 1:1 ligand exchange due to the increased binding strength of phosphonate relative to carboxylate binding groups and the requirement of a proton transfer from free HODPA in solution to bound OA on the surface of the QD in order for the ODPA to bind, as shown in previous studies.[31] This ligand exchange is shown schematically in Figure 2B. Precipitation with anti-solvent and centrifugation is then used to remove free ligands. Upon ligand exchange, there is no change in the absorption spectra of the QDs, verifying that QDs are not being etched by this process. This is shown in the Supporting Information.

To quantify the ligand exchanges, we use proton NMR of the cleaned samples, a technique that has been effectively used in the past to study QD ligand shells.[34,35] NMR was performed in the 20-90 mM of ligand range (about 100-500 μM in QDs). Relatively high concentrations were used to ensure adequate signal of the broadened peaks, and minimize Z-type ligand (Cd-carboxylate or –phosphonate) desorption, which would complicate quantification. As shown in Figure 2A, broadened NMR peaks characteristic of ligands strongly bound to the QD surface were observed. The lack of any sharp peaks, characteristic of free ligand in solution, indicates that the QDs are well purified. The peaks corresponding to the OA vinyl protons (A), the OA protons on the carbon adjacent to the alkene (B), and the methyl protons of both OA and ODPA (C) bound to the QD surface are labeled, as shown in Figure 2A. We do not observe a peak associated with the protons on the alpha carbon for either the ODPA or the OA, likely due to significant broadening of the peak. All other aliphatic protons are within the broad peak at around 1.2 ppm.

The NMR spectra of the QD samples are normalized to the QD concentration using an external standard. Extent of ligand exchange is easily monitored by a decrease in intensity of the vinyl peaks associated with OA relative to the standard. The decrease of peak (A) is shown more clearly in Figure 2A (inset). Peak C does not decrease dramatically, suggesting that there is not a significant stripping of ligands. The normalized ligand density is quantified by peak C and shown in Table 1. To quantify the ligand composition, we fit the peak areas of the methyl peak (C) and the vinyl peak (A) to determine the mole fractions of OA and ODPA, as shown in eq. 1.

$$\frac{3*\text{vinyl peak}}{2*\text{methyl peak}}=x \quad (1)$$

In eq. 1 x is the mole fraction of OA present in the ligand shell, and the 3/2 arises from the different number of methyl and vinyl protons. The observed NMR ratios and resultant ligand shell compositions are shown in Table 1. We assume a 5% error on the ratios for the NMR. In addition, as we normalize the NMR to QD concentration we can determine the relative ligand coverage, compared to the native sample (ODPA36). The error on the ligand coverage measurement is likely high (~10% or so), as an external standard was used for the quantitative NMR. This data is also shown in Table 1. Inductively coupled plasma-atomic emission spectroscopy (ICP-AES) of the Cd^{2+} concentration for nitric acid digested QDs allows for the determination of the extinction coefficient of the QDs, and from that value, determination of the ligand packing density. The ligand packing density observed for sample ODPA36 was 4.9 ($+¿−¿$ 1.1) ligands/nm^2, which is of the correct order of magnitude when compared to similar nanocrystals.[8] The large error bars arise from primarily the quantitative NMR and TEM sizing. For this reason, we mainly report and discuss relative surface coverage for the ligand-exchanged samples. A small decrease in the surface coverage for the three ligand-exchanged samples is observed, although the majority of this occurs for sample ODPA84. The observed decrease in surface coverage is consistent with results from similar ligand exchanges[34,36] and is consistent with preferential stripping of OA due to the presence of trace protic solvents present in the antisolvent.[37] Another possibility is that the ODPA requires more surface area at the QD surface, resulting in fewer ODPA being able to fit on the QD surface.
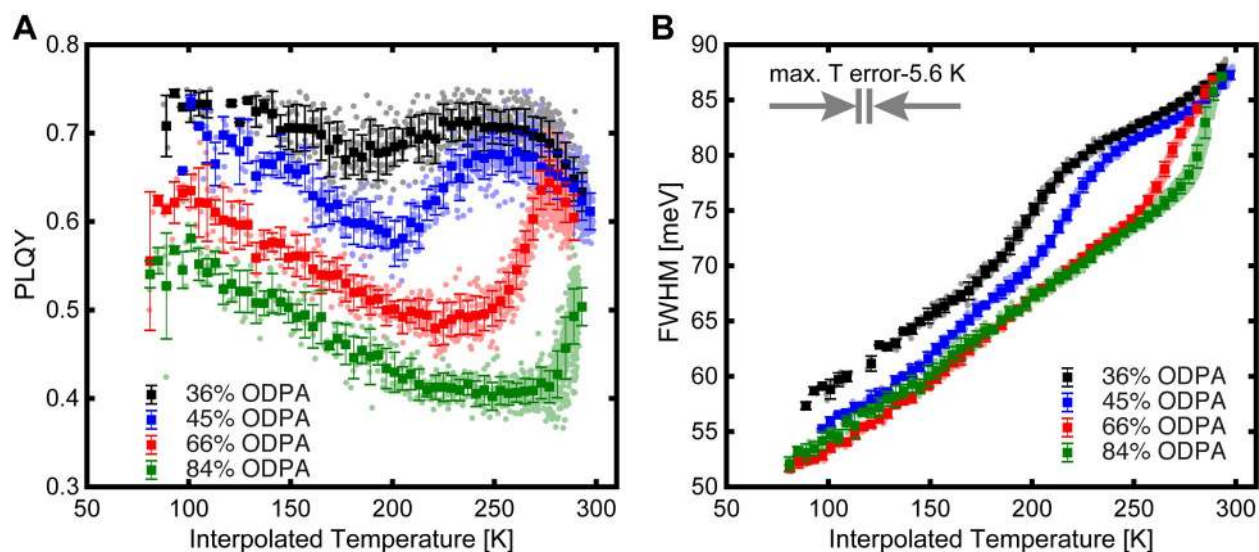
Sample	Percent OA (error)	Percent ODPA (error)	Normalized Ligand Coverage
ODPA36	64 (3)	36 (3)	1
ODPA45	55 (3)	45 (3)	0.95
ODPA66	34 (2)	66 (2)	0.95
ODPA84	16 (1)	84 (1)	0.77

Table 1: NMR quantification of ligand binding

Temperature-dependent photoluminescence

Figure 3: Temperature-dependent photoluminescence measurements of the QD samples. A) shows the PLQY and B) shows the FWHM. The binned data for both is superimposed upon the raw data for clarity. PLQY and FWHM error bars arise from random error due to binning the PLQY and FWHM. The maximum temperature error bar, which arises from the 95% confidence interval for the Newton's law of cooling calibration, is shown in B.

Temperature-dependent PL measurements were performed in an integrating sphere spectrophotometer on both native and ligand-exchanged samples. The sample is flash-frozen in liquid nitrogen, and then data is collected as the sample warms to room temperature using the emission peak and a Newton's law of cooling model to calibrate the internal temperature. This allows us to collect both emission spectra and an absolute PLQY. We chose to perform this absolute measurement rather than a relative measurement due to increased scattering at lower temperatures in the samples, which precludes an accurate relative PLQY measurement. Full details of data analysis and temperature calibration can be found in the Supporting Information. 3-methyl pentane, an organic glass-forming solvent, is used for these measurements to ensure that freezing of the solvent does not change the observed optical properties. The observed trend between PLQY and temperature for all samples is shown in Figure 3A. PLQY is a measure of radiative efficiency and depends on the ratio of radiative and nonradiative rates as shown: $PLQY = \frac{k_r}{k_r + k_{nr}}$, where k_r is the radiative rate and k_{nr} is the nonradiative rate. The PLQY for samples ODPA36, ODPA45, and ODPA66 at room temperature are within error of each other, suggesting that the ligand exchange process did not strip ligands from the surface of the QD. However, for ODPA84, there is a small decrease in the room temperature PLQY value, which supports the conclusion drawn from Table 1, that small amounts of ligand have been stripped from the surface during this ligand

8

exchange process. In all samples a region in which the PLQY increases with temperature, rather than decreases with temperature, is present. This is somewhat unexpected, since nonradiative rates typically increase with increasing temperature resulting in a decrease in PLQY at higher temperatures. A similar phenomenon has been observed and has been correlated with ligand chain length for amine ligands on CdSe QDs, and ascribed to a phase transition within the ligand shell.[10]

Observing an increase in PLQY is, however, insufficient to determine the root cause of the PLQY change. This change could be explained either by an increase in the radiative rate or by a decrease in the nonradiative rate. In previous CdSe/CdS systems, increasing temperature over a similar temperature range was shown to result in a decrease of the radiative rate, which does not fit the observed behavior, but suggests that the radiative rate is mutable over this temperature range.[38,39] To confirm that the nonradiative rate is indeed the changing parameter, temperature-dependent time-resolved photoluminescence experiments were performed on a different QD sample, and are shown in the Supporting Information. In addition, we note that the required optical concentration is lower than that for proton NMR, so the relevance of ligand desorption from the surface should be considered. Concentration-dependent and stearic acid exchange data are shown in the Supporting Information, and indicate that ligand desorption from the surface is not driving the observed behavior.

In addition to observing a temperature dependent change in the PLQY, we see a corresponding change in the full-width at half maximum (FWHM), shown in Figure 3B. In bulk CdSe and nanocrystalline CdSe/CdS the FWHM is known to increase with temperature due to increased thermal population of phonon modes.[38,39] While the exact functional form for the relation between FWHM and temperature is non-trivial, it predicts a smooth increase of FWHM with temperature. However, within the data shown in Figure 3B, there is a clear deviation in the increase with temperature present in the FWHM *versus* temperature curves. This suggests that the ligand phase transition observed impacts both the PLQY and the FWHM. However, the photoluminescence data do not provide insights into the precise nature of the transition we observe. Further characterization is required to better understand the molecular details of this phase transition. Rather than focusing on spectroscopic signatures of the QDs, directly observing the ligand structure would be advantageous. We therefore performed temperature-dependent vibrational spectroscopy focused on the C-H stretching region, as detailed in the following sections.

VT-FTIR Measurements

VT-FTIR measurements were performed on samples ODPA36 and ODPA66, to allow for a structural probe of the phase transition behavior. Measurements were performed in solution in $CDCl_3$ to minimize overlap of solvent and C-H stretching modes, while ensuring QD solubility. Furthermore,

QD concentrations in CDCl$_3$ were comparable to that of the NMR experiments. Therefore, it is expected that all ligands remain bound to the QD surface, as is observed in the NMR data shown in Figure 2A. This allows us to use the methylene stretching frequencies observed to determine qualitative information about the structure of the ligands bound to the QDs. A portion of the C-H stretching region of samples ODPA36 and ODPA66 is shown in Figure 4B-C. Full spectra before and after solvent and baseline subtraction are shown in the SI. There are four peaks present: the symmetric methylene stretch (s-CH$_2$), the symmetric methyl stretch (s-CH$_3$), the antisymmetric methylene stretch (as-CH$_2$), and the antisymmetric methyl stretch (as-CH$_3$). Furthermore, the vinyl C-H stretch decreases in relative intensity from sample ODPA36 to ODPA66, further confirming the ligand exchange shown by the NMR data (see Supporting Information for details).

CH$_2$ stretching frequencies are sensitive to the structural conformations of the aliphatic chains of the ligands. Specifically, the frequency of the s-CH$_2$ and as-CH$_2$ (highlighted in Figure 4B-D) can inform on the conformation of the aliphatic chains, since an increase in stretching frequency corresponds to an increase in the number of *gauche* configurations present in the methylene chain.[40] The all *trans* configuration results in a planar carbon backbone, and would allow for efficient packing of aliphatic chains. Therefore, tracking the CH$_2$ stretching frequency as a function of temperature can serve as a proxy measure of chain packing. Larger stretching frequencies indicate more *gauche*, and therefore more disordered ligands, while smaller stretching frequencies are associated with ordered, more *trans,* ligands. The most common *gauche* C-C defects are described in Figure 4A.[41] These *gauche* defects disrupt the planar carbon backbone and will result in a more disordered ligand shell.
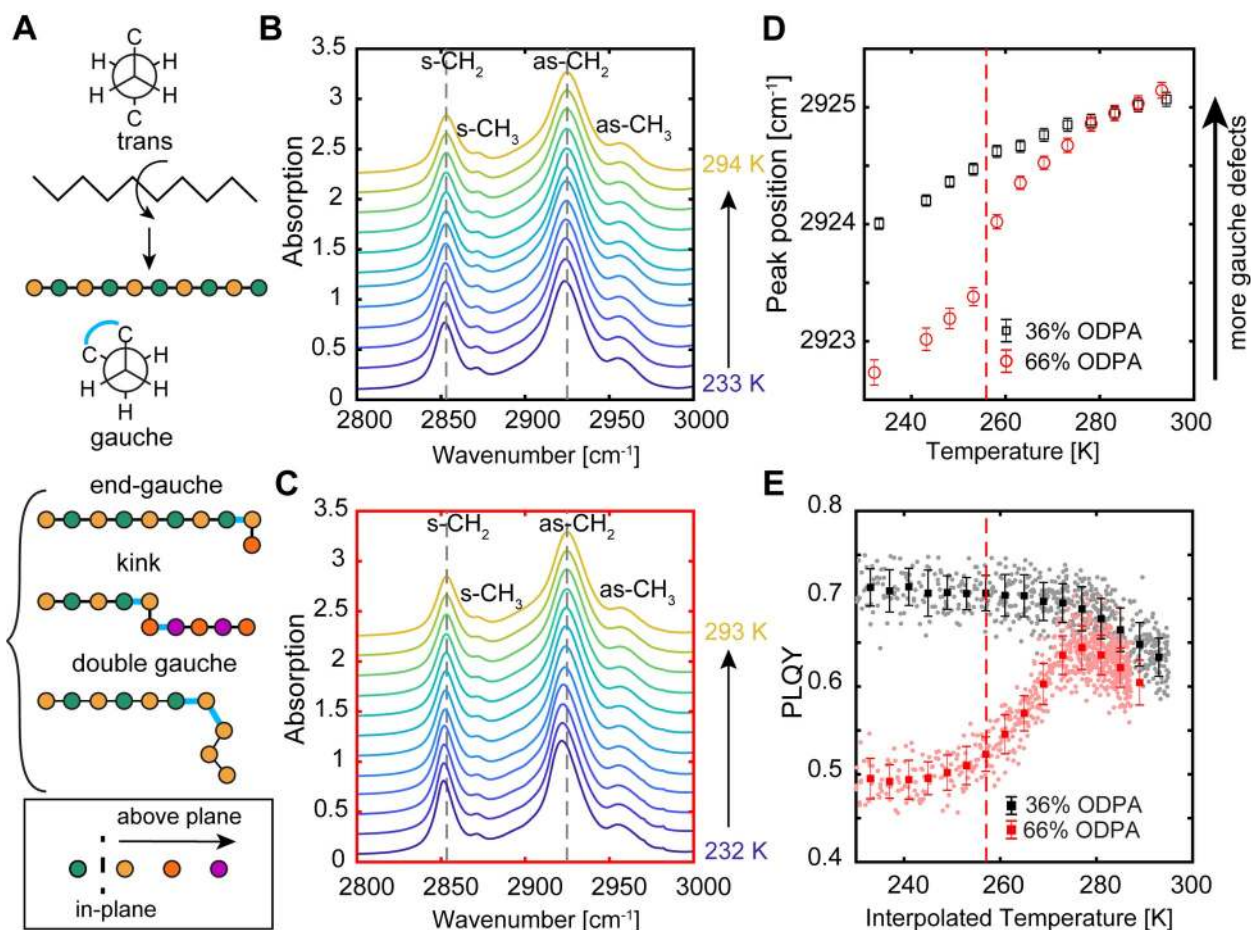
Figure 4: A) shows the structure of *trans* and *gauche* configurations of aliphatic chains. The common *gauche* defects are shown as ball-and-stick models. B) and C) show VT-FTIR of the C-H stretching region for sample ODPA36 and sample ODPA66 respectively. D) and E) compare the antisymmetric C-H stretching peak position with the PLQY data, respectively.

The temperature-dependent as-CH_2 stretching frequencies for ODPA36 and ODPA66 is shown in Figure 4D and the temperature-dependent PLQY data is shown on the same scale in Figure 4E. Both samples show a gradual increase in as-CH_2 stretching frequency as temperature increases, although sample ODPA36 has a higher peak position. At just below the optically observed phase transition temperature for ODPA66, there is a sharp increase in the as-CH_2 stretching frequency as temperature increases for ODPA66 but not for ODPA36. These phase transitions are clearly related, the details of which will be explained in the Discussion. Furthermore, a similar transition is observed in the s-CH_2 (shown in the Supporting Information), but the frequency change for the s-CH_2 stretch is smaller.

The observed magnitude of change for both methylene stretching frequencies is significantly smaller than previous observations in self-assembled monolayers on a variety of substrates[42] and on the (2-3 nm diameter) octadecanethiolate capped Au nanoparticles.[15] Additionally, we observe a higher methylene stretch frequency (more disordered) in the low

11

temperature phase than in the aforementioned other systems. This suggests that the low-temperature, ordered phase in the CdSe/CdS QDs has more disorder present than in the Au-thiolate system, which is further addressed in the Discussion. The VT-FTIR data shows that the phase transition observed through PL spectroscopy is due to a change in the structure of the aliphatic ligand chains, as the increase in *gauche* C-C bonds corresponds to the same temperature. More information on the degree of order in these systems can be gained through SFG spectroscopy.

SFG Spectroscopy

SFG measurements were performed with QDs spun-cast onto a quartz substrate and then immersed in hexanes to ensure ligand solvation remains relatively consistent between the PL, IR, and the SFG measurements. Since SFG is particularly sensitive to order at the interface, it is an effective way to probe the ligand surface structure. We have probed the characteristic aliphatic tail structure vibrations, *i.e.* the methylene backbone (s-CH_2 at 2850 cm^{-1}, as-CH_2 at 2920 cm^{-1}) and methyl end group (s-CH_3 at 2880 cm^{-1}, as-CH_3 at 2960 cm^{-1}) were easily detectable, enabling us to study the order of the ligand aliphatic chains. Other notable bands are the Fermi resonances of the methylene (at 2940 cm^{-1}), and methyl (2950 cm^{-1}) groups, which shift their energies and intensities due to coupling to other vibrations.[43] In addition, as we expect the ordered ligands to stand somewhat perpendicular with respect to the QD surface, the laser beams were polarized to an *SSP* polarization combination (for *S*-SFG, *S*-Vis, *P*-IR).
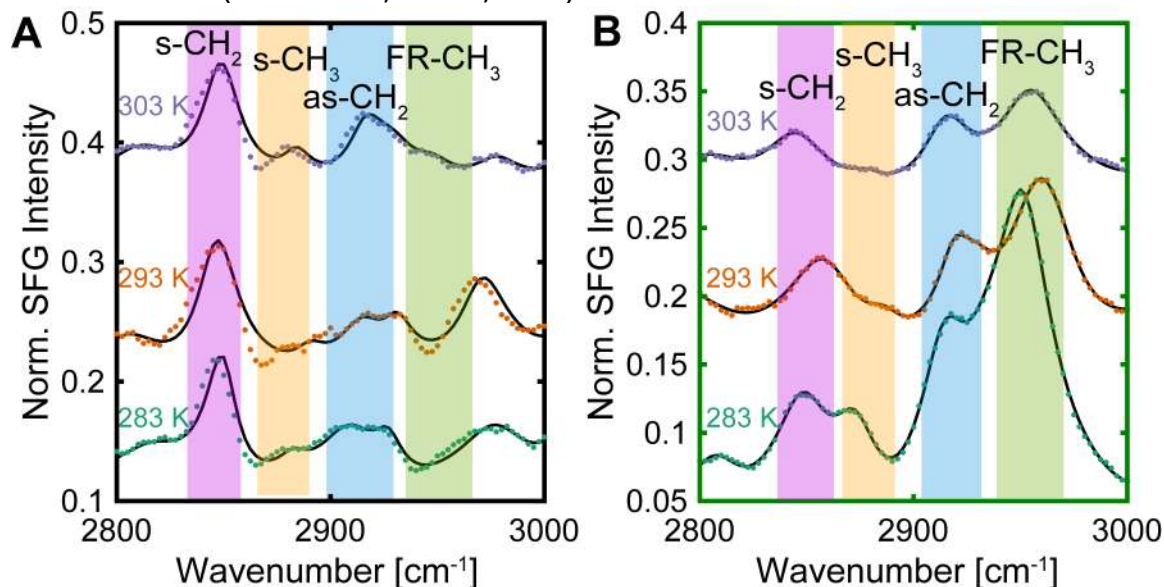
Figure 5: C-H stretching region SFG of QDs at a quartz/hexanes interface as a function of temperature for sample ODPA36 (A) and sample ODPA84 (B), and peak assignments of discussed stretches. The as-CH_3 is obscured by the FR-CH_3 peak but the position and amplitude are shown in the Supporting Information, as are full peak assignments.

The ratio between the symmetric methyl (s-CH$_3$) (highlighted orange in Figure 5) and methylene (s-CH$_2$) (highlighted purple in Figure 5) stretches is diagnostic of the degree of order in the ligand monolayer, so by comparing temperature-dependent SFG spectra performed on samples ODPA36 and ODPA84 information about the ordering of the ligand shell can be obtained. The SFG experiments were run on the two most different ligand ratio systems to emphasize the differences in the low temperature order. In addition, for the temperature range (283-303 K) for our SFG measurements, only sample ODPA84 could have any order. For this reason ODPA84 and ODPA36 were chosen. A higher s-CH$_3$/ s-CH$_2$ peak intensity ratio is indicative of a more ordered ligand shell, as are sharper and stronger peaks. For sample ODPA36, shown in Figure 5A, there is no significant change in the SFG spectra, in both lineshape and peak intensity, over the observed temperature range. The ratio of methylene to methyl stretch is about 10:1, which suggests a disordered ligand shell. This data is in agreement with the observed PL (Figure 3) and IR data (Figure 4B-C), as both suggest that any change in the ligand tail structure would occur at lower temperatures than those accessible for the SFG experiments. On the other hand, the SFG of sample ODPA84 shows a qualitative change in spectral shape, specifically between 283 K and 293 K, the expected temperature regime for a phase transition as observed *via* the PL measurements highlighted in Figure 3. In particular, we find a significant decrease in the s-CH$_3$ stretch intensity as the temperature increases from 283 to 303 K, indicative of disordering of the ligand shell. This suggests a somewhat ordered configuration at 283 K, as equal methylene and methyl amplitudes is consistent with approximately one *gauche* defect per aliphatic chain (excluding the OA *cis* double bond).[44,45] In fact the 303 K spectra of both samples ODPA36 and ODPA84 are quite similar, suggesting that at this temperature the structure of the ligand shell of both samples is similar. The s-CH3/s-CH2 ratio is a useful parameter that describes the degree of order in the aliphatic chain, and is shown in the Supporting Information to further confirm the presence of a phase transition within sample ODPA84 and not in sample ODPA36 at around 283-293 K.

In addition to the symmetric stretches, analysis of the CH$_3$ Fermi resonance and as-CH$_2$ peaks can yield more information about the structure of the ligand shell. Qualitatively, there is a significant difference in this region between sample ODPA36 and sample ODPA84. In particular, for sample ODPA84, there is a clear increase in the FR-CH$_3$ peak at 283 K compared to sample ODPA36 and other temperatures. An increase in the relative intensity of a Fermi resonance is attributable to a higher degree of similarity between the two modes. For example, tighter packing of neighboring aliphatic tails induce their tails to stretch to their full (all *trans*) length. This in turn can give rise to coupling between a fundamental vibration and the overtone of another vibration (*e.g.*, a C-H stretching mode coupled with a deformation one). Therefore, enhancement of the Fermi resonance in the 283 K, ODPA84, sample is consistent with increased order

(more *trans* conformations) in the ligand shell for this sample. Additionally, the relationship between the s-CH_2 and as-CH_2 can also yield information about the tilt angle of the aliphatic chains, but as shown in the SI, no significant trend can be discerned. This is potentially due to the isotropic arrangement of ligands, which inhibits such an analysis. However, in total, the SFG data performed on sample ODPA84 complements the structural picture we derived from the VT-FTIR analysis of sample ODPA66: an increase in *gauche* defects in the aliphatic chains consistent with an order/disorder type of phase transition occurs at a similar temperature as the transition in PL, as shown in Figure 3.

Composition-dependent behavior

The FTIR and SFG spectroscopies show a clear correlation between the change in the PL properties of the QDs and the structure of the ligand shell. Due to the large change and higher temperature resolution of the photoluminescence properties, we can treat both the PLQY and the FWHM as order parameters that give insight to the extent of the phase transition. In order to better analyze the phase transition temperature and the associated transition width, we fit both the PLQY and FWHM data to the integral of the Cauchy distribution superimposed on a linear change in temperature:

$$O(T) = O_o + bT + c \tanh\left(\frac{T - T_{PT}}{\Delta T}\right) \quad (2)$$

where $O_o + bT$, approximates the change in PLQY and FWHM with temperature excluding the phase transition, which are expected to have more complicated functional forms.[38,39] The parameters c, T_{PT}, and ΔT refer to the strength of the transition, the phase transition temperature, and the width of the phase transition, respectively. Although the use of the integral of the Cauchy distribution to approximate the finite phase transition is somewhat arbitrary, it should capture the essential features of the phase transition.
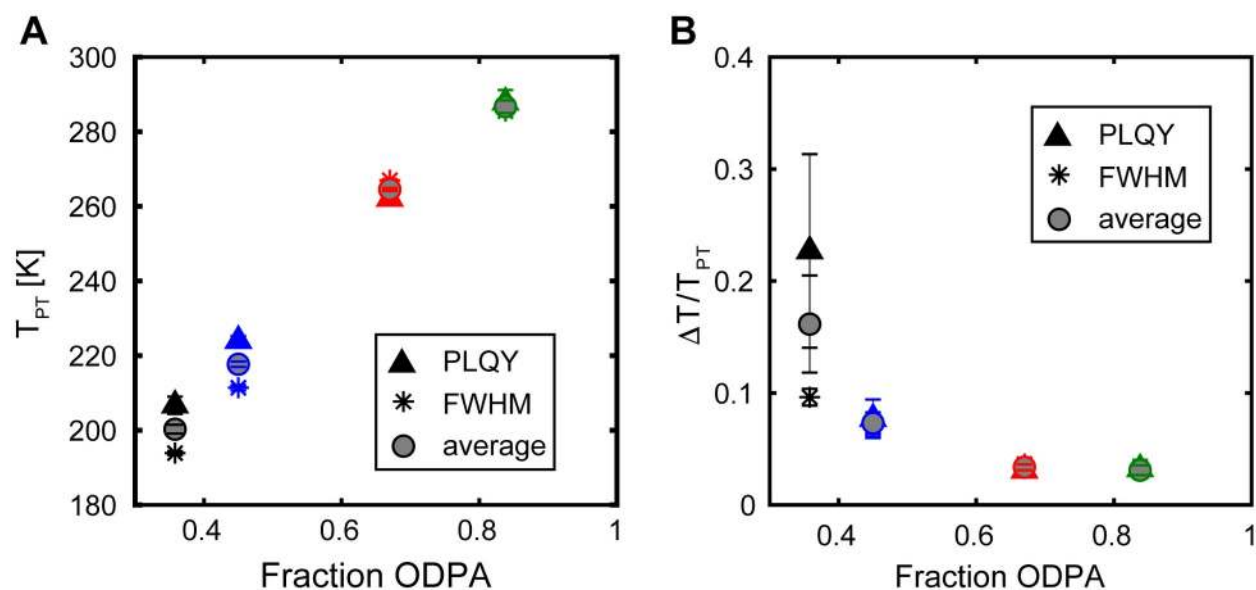
Figure 6: Phase transition temperature (A) and width (B) as a function of ligand composition determined using equation 2.

The PLQY and FWHM data as a function of temperature were fit to eq. (2) and the extracted transition temperatures and normalized peak widths are shown in Figure 6A-B as a function of ligand shell composition (full fits are shown in the Supporting Information). We note that although the use of eq. 2 matches well with phase transition temperatures extracted using a numerical derivative (shown in the Supporting Information), suggesting that this model is reasonable. It is clear that the phase transition temperature increases and the phase transition width decreases with increasing ODPA composition, covering a broad range of values over the samples studied. The phase transition temperature changes by almost 90 K, while the phase transition width changes by about a factor of three. The PLQY and the FWHM data match quite well for all samples except for sample ODPA36, in which there is a significant difference between the observed phase transition widths, likely due to the large error present in the PLQY for sample ODPA36, which has the smallest change in PLQY. However, the FWHM data for sample ODPA36 shows no more error than for the ligand-exchanged samples. In addition, to evaluate the accuracy of the fitting method we compare the phase transition temperatures determined using eq. (2) with the maximal derivative of the binned data, shown in the Supporting Information, and the two show reasonable agreement.

The extracted T_{PT} and $\Delta T/T_{PT}$ can be used to determine how the presence of OA facilitates the observed order/disorder transition. One possibility is that the OA play a minimal role in changing the phase transition and that what dictates the phase transition behavior is the total number of ODPA present in the system, N_{ODPA}. It is well established that for first order phase transitions decreasing the size of the system (number of molecules involved) will result in a decrease in the phase transition temperature (T_{PT}) and a broadening of the phase transition ($\Delta T/T_{PT}$). For a first order transition,

15

both parameters (T_{PT} and $\Delta T/T_{PT}$) are expected to vary in proportion with $1/N_{ODPA}$ or 1/fraction ODPA.[46,47] The behavior shown in Figure 6 does appear to be qualitatively different from this model (it is plotted proportionally to N_{ODPA}). In addition, the large change in the phase transition temperature observed here is inconsistent with previous observations in finite-size systems. For example, in the Au-dodecanethiolate system a change in the number of surface ligands by about a factor of four results in only a 14 K decrease in the phase transition temperature.[48] Similar analysis of ODPA on CdS shows a decrease of approximately 40 K for a ~13-fold change in particle surface area, mainly attributed to an increased surface curvature.[12] This suggests that the OA chains are playing a more active role in disrupting the ODPA chain packing. To describe this behavior, a simple lattice model of the phase transition is developed.

Lattice model of the phase transition

To better explain the observed transition, we can use a simple model that describes the interactions between ODPA and OA chains in both the disordered and ordered states. While complex molecular dynamic simulations are able to most accurately describe the true behavior of such systems, simplified models are of use in providing qualitative understanding, which we use here. As mentioned in the introduction, the ligand phase transition we observe is similar to the gel-to-liquid transition present in phospholipid bilayers. This gel-to-liquid transition can be mapped onto the Ising model using a trigonal lattice, where spin-up is the ordered phase, and spin-down is the disordered phase.[17,18] In the simplest case, the model assumes an energy difference, ϵ, between the ordered and disordered phase. There is a coupling term, W, that accounts for favorable inter-chain coupling only when both chains are ordered. Coupling between two disordered chains or a disordered and an ordered chain is approximated as zero. Finally, there is an associated entropy of the disordered state, S, that can then be mapped to a temperature-dependent field.

These parameters can be directly related to an order/disorder transition within a surface monolayer of QDs. In the model used here, we assume a square lattice both for simplicity and because the Cd sublattice geometry is different on the various w-CdS facets likely present in the QDs. This is sufficient to describe the order/disorder transition within a ligand shell composed entirely of ODPA ligands. In order to simulate the presence of OA within the ligand shell, a given fraction of fixed disordered phase ligands, which represent the bound OA, are introduced randomly within the simulations. This is a reasonable approximation, because OA cannot order in an all *trans* configuration due to the *cis* double bond between carbons 9 and 10.
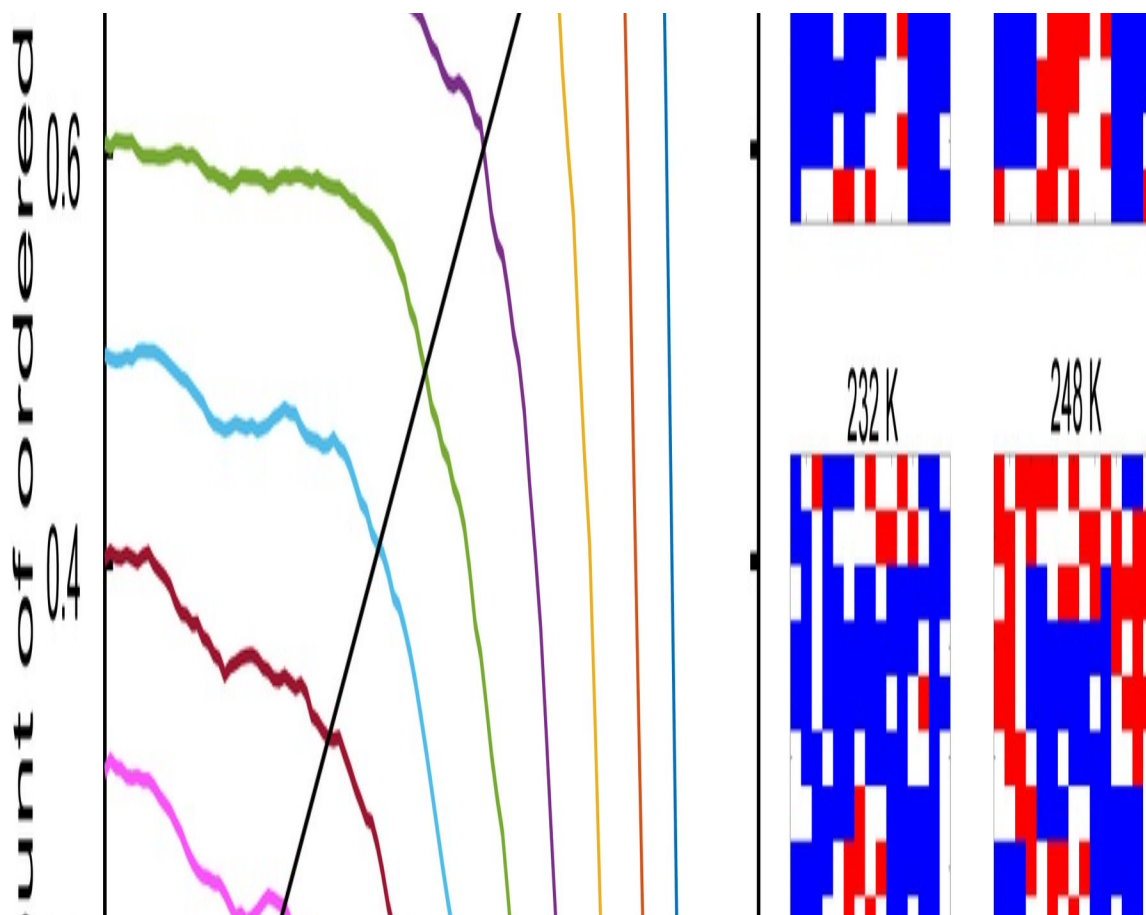
Figure 7: Phase transition model simulations A) shows the amount of order as a function of temperature for eight different compositions. Phase transition temperature (B) and width (C) as a function of amount of ODPA are also shown. The remainder of the ligand shell is composed of OA. D) Microscopic snapshots of the phase transition at different temperatures. Each square corresponds to a single molecule. The blue corresponds to ordered ODPA, the red to disordered ODPA, and the white to OA. This sample used a 70% ODPA configuration.

The three parameters involved in this simulation are inter-related and likely different combinations of these parameters could result in similar model outcomes. A further discussion on how varying the model parameters changes the phase transition behavior is described in the Supporting Information. However, the values chosen here were both based on prior work and have physical meaning. The energy spacing, ε, is 109.5 meV and corresponds to the energetic cost of forming *gauche* defects to "melt" the aliphatic chains. The energetic cost of one *gauche* defect is approximately 40 meV[49] so the chosen value accounts for on average slightly more than two *gauche* defects in the aliphatic chains. In addition, there is a change in the volume of the ligand shell, which in the lipid bilayers translates to a 19.5 meV enthalpy change per site.[17,18] The coupling energy between ordered

ODPA chains, W, is derived from the van der Waals interaction between two packed aliphatic chains. In close-packed stearic acid this energy is approximately 360 meV,[50] but in this work 140 meV was chosen as it matches better with the experimental results (see SI for details). Due to both the surface curvature of the QD and the fact that the inter-ligand spacing (which arises from the spacing of the underlying Cd sub-lattice) is greater than in close-packed stearic acid, this value is reasonable.[50,51] The coupling parameter was varied to better match the experimental results, and simulations with different couplings are shown in the Supporting Information. Finally, we use an entropy S of 14.6 k_B, which corresponds to a degeneracy of several hundred thousand different chain configurations for the disordered phase. While this value is quite high, there is a significant increase in configurational entropy as well as positional entropy upon chain melting. Furthermore previous experimental studies on lipid bilayer melting have shown that the order-disorder phase transition in those systems has an associated change in entropy of 14.6 k_B, which is why that number is used here.[17]

The results of simulating compositions consisting of 30% to 100% ODPA are shown in Figure 7A-C. As observed in the PL measurements shown in Figure 3, as the concentration of ODPA in the ligand shell increases, the phase transition shifts to higher temperatures and narrows in width. The degree of asymmetry in the phase transition also appears to vary with ODPA composition, with the simulations with less ODPA resulting in a more asymmetric phase transition, in which the initial decrease in order is more gradual than the final disordering process. The temperature range of the phase transition, which varies over approximately 150 K for the compositions studied, shows a similar qualitative trend as the experimental results. The trend in describing the phase transition width generally matches the experiment, but the FWHM underestimates the phase transition width for sample ODPA36 as compared to the simulation.

The general agreement between the model and the experimental results suggests that OA molecules act as local points of disorder that drive the observed phase transition. This agreement, allows us to use the developed model to gain microscopic insights into the nature of the phase transition. Shown in Figure 7D are snapshots in temperature of a configuration with 70% ODPA. At low temperatures, randomly distributed OA seed small disordered domains. This results in the phase transition propagating outward from regions with more OA as the temperature is increased. The regions in which there is the least amount of OA require the highest temperature to disorder. This also explains the slight asymmetry shown in the phase transition in Figure 7A. The shape of the phase transition is somewhat sharp as the system completely disorders, whereas during the initial melting there is a more gradual disordering, which is most evident in the samples with 30 and 40% ODPA in Figure 7A. This can be explained by the fact that there is more variation in the environments of the ordered ODPA chains at the beginning of the phase transition than at the end,

resulting in an asymmetric phase transition profile that is not present in the 100% ODPA case.

Origin of the change in PL at the ligand phase transition

The systematic study of the order/disorder transition in mixed ligand shells using both PL and IR spectroscopies presented here suggests several key areas for further analysis. In particular, we desire to gain a better understanding of how the ligand phase transition can impact the QD PL properties, understand discrepancies between the PL and VT-FTIR measurements, compare the transition observed here to other systems, and determine what model parameters are necessary to account for the observed phase transition. We will first discuss the origin of the observed change in PL properties. Both this work and that of several other groups now indicate that a transition in the optical properties correlates with a change in the ligand aliphatic chains.[10,27] Similar effects occur for systems that have amine binding groups as well as those that have a mix of carboxylate and phosphonate binding groups. There is therefore some universality in the mechanism, as it occurs across a number of binding groups and even across two different binding motifs (X-type carboxylates and phosphonates, and L-type amines).[10,27] Taken together, this suggests that the mechanism of trap formation is one that could occur for a number of binding group geometries. One potential explanation is that the change in aliphatic chain conformation also changes the energy of surface trap states.

A change in binding group orientation is one factor that could modulate the energy of surface traps. The preferential orientation of the ligand chains, which arises when the aliphatic chains are ordered, thus induces an effective strain at the inorganic/organic interface, analogous to the strain that arises at an interface between two geometric lattice mismatched materials. This would likely result, to some degree, in a change in binding geometry of the ligand head group to the nanocrystal surface. We could consider the change in binding geometry to be primarily due to a changing binding angle. However, there is an additional possibility of a change in binding mode (for example a binding in a chelate *versus* a bridging fashion), resulting in different surface passivations.[52] Both of these changes in binding geometry would likely result in the emergence of a trap state as the binding configuration of the head groups is changed. A related phenomenon would be a change in binding group orientation changing the QD surface dipole and therefore shifting the band edges relative to a surface trap.[53]

Coupling between the exciton and surface ligands can also explain the observed trend in the FWHM: increasing upon ligand disordering. Due to the thin shell, the exciton can couple to surface states. This results in the potential for fluctuations in ligand binding to impact the QD optical properties. When the ligands are ordered, the ligand binding geometry is fixed by the ordering of the aliphatic chains; however, when the ligands are disordered we would expect greater fluctuations in binding configurations,

resulting in a broader emission spectrum. Computational work has shown that for small CdSe QDs, the presence of ligands can result in as much as a factor of two decrease in the homogeneous photoluminescence linewidth due to a decrease in fluctuations of the inorganic atoms, so a variety of binding configurations could result in a small change in the observed photoluminescence linewidth.[54]

Understanding structural changes in the ligand shell

In addition to developing a better understanding of the change in PL properties due to the ligand phase transition, further analysis of the vibrational and PL spectroscopies can improve our molecular picture of the observed phase transition. For example, there is a small difference between the observed phase transition temperature for the VT-FTIR and the PL data. The VT-FTIR data indicates that the ligand phase transition occurs slightly below the temperature observed for the PL properties (Figure 4D). The PL data is likely to be more sensitive to changes closer to the QD surface, and a previous computational study on Au-dodecanethiolate nanocrystals has shown that as temperature is increased, more gauche defects form on the outer carbons of aliphatic chains compared to the inner carbons.[48] This would result in the VT-FTIR measurements, which are sensitive to the majority of the bonds in the aliphatic chains, to predict a slightly lower phase transition temperature than the PL data, which are more sensitive to the structure near the surface of the QD. While it is difficult to assign a particular phase transition temperature for the SFG of sample ODPA84, the observed change in SFG signature coincides with the extracted phase transition temperature. It is possible that due to the sharper nature of the phase transition for sample ODPA84 the discrepancy between an average measurement of the aliphatic chains and a measurement more sensitive to the surface is less. Similarly, the difference in phase transition width between the experiment and the simple model could partially be due to the failure of the model to take into account the fact that the phase transition occurs at slightly different temperatures along the aliphatic chain, as mentioned above.

Information about the strength of the phase transition can also be extracted from the IR spectroscopies performed. The observed change in the as-CH_2 stretch position (Figure 4D), is smaller than in other systems.[15] This observation is complemented by the SFG data (Figure 5B), which shows significant s-CH_2 amplitude even in the ordered phase (283 K), also suggesting that there is significant disorder present in the ordered phase. One possibility is that the small particle size, which results in variable faceting present in these particles reduces the ordering through an increase in chain defects at the facet edges, as has been observed previously in platelet systems[45] and is similarly shown to be more prominent for smaller diameter QDs.[55] Furthermore, the larger spacing between the Cd sub-lattice when compared to elemental materials could also result in more disorder present in the "ordered" phase due to weaker coupling between the aliphatic

chains. This is of particular note, as the structure of the ligand shell has been shown to impact solubility in a variety of nanocrystal systems.[9,19,20] In order to maximize solubility, as has been suggested in previous systems, the ligand shell should be compatible with the organic solvent but also should not order into bundled domains. This can be achieved in a number of ways, including by using branched ligands,[19] or as is indicated within this work, by including a ligand with a *cis* double bond that prevents packing of straight chain ligands. Furthermore, the model suggests that short aliphatic chains, or unpassivated surface sites would also modify the observed phase transition within the ODPA in the same manner, which is in accord with previous computational studies of the effect of surface coverage on the ligand phase transition.[12]

The assumptions used in developing the Ising model can also give insight into the structure of the ligand shell. As shown in Figure 7, a model that includes randomly distributed OA maps reasonably well to the experimental results. In fact, if complete phase segregation is assumed, the phase transition behavior does not match the experimental results, as shown in the Supporting Information. This would also suggest that over the course of the phase transition, the ODPA and OA remain randomly distributed. The random distribution of OA and ODPA also implies that the binding of the ligand to the surface is more important in determining the distribution of ODPA and OA within the ligand shell than the inter-ligand interactions. As the ligand exchange is performed above the phase transition temperature, it is likely that the entropy of mixing outweighs enthalpic segregation between the ODPA and the OA, which is consistent with experiments observing ligand segregation in nanoparticle systems.[56]   The presence of OA that is well-mixed within the ODPA is important, since if the two ligands were segregated, it would be harder for small amounts of OA to have significant impacts on the phase transition behavior of the ligand shell.

Conclusions:

This study demonstrates how the introduction of OA can disrupt the packing of ODPA chains in the ligand shell of CdSe/CdS QDs. By controlling the amount of OA present in the ligand shell, the order/disorder phase transition that occurs within the ODPA can be modified, as small domains of OA seed disorder within the ODPA ligands. In this work, the phase transition is studied using both PL and IR techniques (FTIR and SFG spectroscopy). The observed change in PLQY and FWHM allows us to precisely determine the phase transition temperature and width. The VT-FTIR and SFG studies are critical in providing us further understanding of the molecular details of the phase transition, for which the PL data only provides indirect evidence. The composition-dependence of the phase transition temperature and the phase transition width is then analyzed using a simple Ising-derived model of the phase transition, which shows that the phase transition is occurring among the ODPA chains, and is actively disrupted by the OA chains. This study

highlights the importance of fully understanding the structure-property relationships inherent to the ligand shell structure. In addition to modulating the PL, the ligand shell structure can impact properties such as inter-QD interactions and the permeability of the ligand shell, which are relevant properties in a number of potential QD applications.

Methods/Experimental:

Chemicals:
cadmium oxide (CdO, ≥99.99%), selenium (Se 99.99%), tri-*n*-octylphosphine oxide (TOPO,99%),oleic acid (HOA,90%), 1-octadecene (ODE, 90%) were purchased from Sigma-Aldrich. Octadecylphosphonic acid (HODPA, 99%, PCI Synthesis) and tri *n*-octylphosphine (TOP, 99%, STREM) were also used. Anhydrous solvents hexanes, acetone, tetrahydrofuran (THF), and 3-methylpentane were used as received.

QDs were synthesized using a modified literature preparation.[30,32] Both the core synthesis and the shelling procedure are briefly described below.

CdSe core synthesis:
120 mg CdO, 560 mg of HODPA, and 6 g TOPO were combined in a 25 mL three-neck round bottom flask. The mixture was heated to 150 °C and placed under vacuum until the line reached its base pressure (~20 minutes). The flask was then placed under Ar and heated to 325 °C until it turned transparent. The flask was then cooled to 150 °C, and placed under vacuum until the line reached its base pressure (several minutes). It was then placed under Ar and heated to 325 °C at which point 2 mL of TOP were injected. The mixture was then heated to ~372 °C and 118 mg of Se dissolved in 1 mL of TOP was swiftly injected. Different core sizes can be synthesized by modulating injection temperature and growth time. The reaction was allowed to grow for about 50 s before being cooled. 4 mL toluene was injected as the solution cooled, and the QDs were cleaned with successive precipitation with acetone and redispersion in hexanes.

CdSe/CdS synthesis:
700 nmol of CdSe cores (determined using absorption[57]) were added to 40 mL of ODE under Ar. The mixture was then degassed for an hour and then heated up to 110 °C for 20 minutes under vacuum. 4.9 mL 0.2 M Cd-oleate (10.25 HOA: 1 cadmium) and 4.9 mL 0.2 M 1-octanethiol in ODE were then injected at 10.5 mL/hr under Ar as the solution was heated to 310 C. After the injection was completed, the solution was kept at 310 °C for 30 minutes before being cooled to room temperature. QDs were cleaned with successive precipitation with acetone and redispersion in hexanes. They were stored in an Ar environment dissolved in approximately 5 mL of hexanes.

Ligand exchanges:
A sub-stoichiometric amount of HODPA was added to a dispersion of QDs (800 μL of stock solution) in 20 mL of THF. The solution was stirred for one hour, and then concentrated to ~3 mL of THF. The solution was cleaned twice with THF/acetone and once with hexanes/acetone. The ligand composition was then measured with quantitative NMR in $CDCl_3$ on a Bruker 400 MHz NMR, using an external standard of 9.8 mM ferrocene in toluene-d_8.

Measuring the surface ligand density:
A number of techniques are required to measure the surface ligand density. The concentration of Cd^{2+} ions in a sample of QDs was measured using an Optima 7000 DV ICP-AES. ICP was performed on dilutions of a sample of QDs digested with concentrated nitric acid, referenced to a Cd standard, and then correlated with an absorption measurement. The surface area of a QD is then determined using TEM. These measurements can then be correlated with the quantitative NMR measurement described above. The resultant error analysis includes random error associated with the quantitative NMR and TEM sizing (approximately 10% each).

Temperature-dependent PLQY:
QDs were added to 0.4 mL of 3-methylpentane in an NMR tube, such that the O.D. at 500 nm was approximately 0.2 (approximately 50x dilution from NMR concentrations). The NMR tube was flame-sealed, and PLQY with a 500 nm excitation were taken in an integrating sphere setup.[58] Samples were flash frozen in liquid N_2 and data was collected as they warmed in the integrating sphere. We use the emission peak wavelength (measured externally in a cryostat) and a Newton's law of cooling model to determine the temperature of the sample.

Variable-Temperature FTIR:
QDs were dried and then redispersed in $CDCl_3$ such that the ligand concentration was approximately 20 mM. This was loaded into a 500 μm path length Specac Variable Temperature IR cell with CaF_2 windows. FTIR data were collected on a Nicolet 6700 FT-IR Spectrometer upon warm-up.

SFG vibrational spectroscopy:
Quartz substrates were prepared by cleaning with Nochromix solutions and then successive washings with water, IPA, and toluene. QDs were deposited *via* spin-coating from a ~200 nM solution of QDs in toluene. The picosecond laser system consisted of a 1064 nm Nd:YAG pump laser (PL2230, Ekspla) with a repetition rate of 50 Hz and an average peak power of 25 mJ. A LaserVision optical parametric generator and amplifier system converted the 1064 nm to a visible 532 nm beam and a mid-IR beam ranging between 2200 and 4000 cm^{-1}. The visible and infrared beams overlap spatially and temporally on a medium. The beam angles were 34° and 48°, respectively, regarding the perpendicular plane to the sample surface (reference plane).

We collected the SFG beam (in the UV range) by a Hamamatsu photomultiplier tube. We added several band-pass filters to minimize stray 532 nm light. Unless specified differently, we used an SSP (SFG, vis, IR) polarization combination because it is sensitive to the adsorbate dipole moment perpendicular to the interface. The temperature was controlled *via* a commercial heater having a PID control unit to maintain a constant temperature. The cooling was carried out by attaching special cooling packs that engulfed the air-tight SFG cell. We applied a common practice in which by controlling the heating rate against a low temperature sink we were able to achieve constant temperature for hours long. The temperature was measured by two sets of type K thermocouples. One was attached to the bottom of the liquid SFG cell and the second was attached by an adhesive Kapton film to the CaF_2 window.

Ising Model Simulations:
The Ising model used was implemented in Matlab, with 10^7 Monte Carlo steps using the Metropolis sampling algorithm to ensure the system reached equilibrium. The lattice simulated was a 15x15 square lattice, which would correspond to a surface coverage of 2-3 ligands/nm^2 for the QDs studied. 20 different OA configurations were averaged over for each data point in order to account for variation in the phase transition properties depending upon the random configuration of OA in the sample.

Associated Content:
Supporting Information: Absorption, emission, TEM, time-resolved photoluminescence measurements, PLQY processing data, IR data processing steps, $CDCl_3$ IR background at different temperatures, SFG fit parameters, binning PLQY + FWHM data, fits for determining T_{PT} and ΔT, details of the lattice model, and fitting parameters. This material is available free of charge *via* the Internet at http://pubs.acs.org.
The authors declare no competing financial interests.

Author Information:

Corresponding Author
*E-mail: paul.alivisatos@berkeley.edu

Present Address
‡School of Chemistry, Faculty of Exact Sciences, Tel Aviv University, Tel Aviv 6997801, Israel

ORCID
Arunima D. Balan: 0000-0002-9216-7806
Jacob H. Olshansky:0000-0003-3658-1487
Yonatan Horowitz: 0000-0002-7150-9264
Erin A. O'Brien: 0000-0002-3448-2402

Gabor A. Somorjai: 0000-0002-8478-2761
A. Paul Alivisatos: 0000-0001-6895-9048

Acknowledgments:

References:

(1)   Medintz, I. L.; Uyeda, H. T.; Goldman, E. R.; Mattoussi, H. Quantum Dot Bioconjugates for Imaging, Labelling and Sensing. *Nat. Mater.* **2005**, *4*, 435–446.

(2)   Zrazhevskiy, P.; Sena, M.; Gao, X. Designing Multifunctional Quantum Dots for Bioimaging, Detection, and Drug Delivery. *Chem. Soc. Rev.* **2010**, *39*, 4326–4354.

(3)   Boles, M. A.; Ling, D.; Hyeon, T.; Talapin, D. V. The Surface Science of Nanocrystals. *Nat. Mater.* **2016**, *15*, 141–153.

(4)   Lee, J.-S.; Kovalenko, M. V; Huang, J.; Chung, D. S.; Talapin, D. V. Band-like Transport, High Electron Mobility and High Photoconductivity in All-Inorganic Nanocrystal Arrays. *Nat. Nanotechnol.* **2011**, *6*, 348–352.

(5)   Kovalenko, M. V.; Bodnarchuk, M. I.; Zaumseil, J.; Lee, J. S.; Talapin, D. V. Expanding the Chemical Versatility of Colloidal Nanocrystals Capped with Molecular Metal Chalcogenide Ligands. *J. Am. Chem. Soc.* **2010**, *132*, 10085–10092.

(6)   Pu, C.; Peng, X. To Battle Surface Traps on CdSe/CdS Core/Shell Nanocrystals: Shell Isolation *versus* Surface Treatment. *J. Am. Chem. Soc.* **2016**, *138*, 8134–8142.

(7)   Gao, Y.; Peng, X. Photogenerated Excitons in Plain Core CdSe Nanocrystals with Unity Radiative Decay in Single Channel: The Effects of Surface and Ligands. *J. Am. Chem. Soc.* **2015**, *137*, 4230–4235.

(8)   Anderson, N. C.; Hendricks, M. P.; Choi, J. J.; Owen, J. S. Ligand Exchange and the Stoichiometry of Metal Chalcogenide Nanocrystals:

Spectroscopic Observation of Facile Metal-Carboxylate Displacement and Binding. *J. Am. Chem. Soc.* **2013**, *135*, 18536–18548.

(9)   Monego, D.; Kister, T.; Kirkwood, N.; Mulvaney, P.; Widmer-Cooper, A.; Kraus, T. Colloidal Stability of Apolar Nanoparticles: Role of Ligand Length. *Langmuir* **2018**, *34*, 12982–12989.

(10) Wuister, S. F.; Van Houselt, A.; De Mello Donegá, C.; Vanmaekelbergh, D.; Meijerink, A. Temperature Antiquenching of the Luminescence from Capped CdSe Quantum Dots. *Angew. Chemie - Int. Ed.* **2004**, *43*, 3029–3033.

(11) Widmer-Cooper, A.; Geissler, P. Orientational Ordering of Passivating Ligands on CdS Nanorods in Solution Generates Strong Rod-Rod Interactions. *Nano Lett.* **2014**, *14*, 57–65.

(12) Widmer-Cooper, A.; Geissler, P. L. Ligand-Mediated Interactions between Nanoscale Surfaces Depend Sensitively and Nonlinearly on Temperature, Facet Dimensions, and Ligand Coverage. *ACS Nano* **2016**, *10*, 1877–1887.

(13) Luedtke, W. D.; Landman, U. Structure, Dynamics, and Thermodynamics of Passivated Gold Nanocrystallites and Their Assemblies. *J. Phys. Chem.* **1996**, *100*, 13323–13329.

(14) Ghorai, P. K.; Glotzer, S. C. Molecular Dynamics Simulation Study of Self-Assembled Monolayers of Alkanethiol Surfactants on Spherical Gold Nanoparticles. *J. Phys. Chem. C* **2007**, *111*, 15857–15862.

(15) Badia, A.; Cuccia, L.; Demers, L.; Morin, F.; Lennox, R. B. Structure and Dynamics in Alkanethiolate Monolayers Self-Assembled on Gold Nanoparticles: A DSC, FT-IR, and Deuterium NMR Study. *J. Am. Chem. Soc.* **1997**, *119*, 2682–2692.

(16) Fenter, P.; Eisenberger, P.; Liang, K. S. Chain-Length Dependence of the Structures and Phases of $CH_3(CH_2)_{n-1}SH$ Self-Assembled on Au(111). *Phys. Rev. Lett.* **1993**, *70*, 2447–2450.

(17) Doniach, S. Thermodynamic Fluctuations in Phospholipid Bilayers. *J. Chem. Phys.* **1978**, *68*, 4912–4916.

(18) Mouritsen, O. G.; Boothroyd, A.; Harris, R.; Jan, N.; Lookman, T.; MacDonald, L.; Pink, D. A.; Zuckermann, M. J. Computer Simulation of the Main Gel–Fluid Phase Transition of Lipid Bilayers. *J. Chem. Phys.* **1983**, *79*, 2027–2041.

(19) Yang, Y.; Qin, H.; Jiang, M.; Lin, L.; Fu, T.; Dai, X.; Zhang, Z.; Niu, Y.; Cao, H.; Jin, Y.; Zhao, F.; Peng, X. Entropic Ligands for Nanocrystals: From Unexpected Solution Properties to Outstanding Processability. *Nano Lett.* **2016**, *16*, 2133–2138.

(20) Kister, T.; Monego, D.; Mulvaney, P.; Widmer-Cooper, A.; Kraus, T. Colloidal Stability of Apolar Nanoparticles: The Role of Particle Size and Ligand Shell Structure. *ACS Nano* **2018**, *12*, 5969–5977.

(21) Wang, Z.; Schliehe, C.; Bian, K.; Dale, D.; Bassett, W. A.; Hanrath, T.; Klinke, C.; Weller, H. Correlating Superlattice Polymorphs to Internanoparticle Distance, Packing Density, and Surface Lattice in Assemblies of PbS Nanoparticles. *Nano Lett.* **2013**, *13*, 1303–1311.

(22)	Nienhaus, L.; Wu, M.; Geva, N.; Shepherd, J. J.; Wilson, M. W. B.; Bulović, V.; Van Voorhis, T.; Baldo, M. A.; Bawendi, M. G. Speed Limit for Triplet-Exciton Transfer in Solid-State PbS Nanocrystal-Sensitized Photon Upconversion. *ACS Nano* **2017**, *11*, 7848–7857.

(23)	Geva, N.; Shepherd, J. J.; Nienhaus, L.; Bawendi, M. G.; Van Voorhis, T. Morphology of Passivating Organic Ligands around a Nanocrystal. *J. Phys. Chem. C* **2018**, *122*, 26267–26274.

(24)	Weinberg, D. J.; He, C.; Weiss, E. A. Control of the Redox Activity of Quantum Dots through Introduction of Fluoroalkanethiolates into Their Ligand Shells. *J. Am. Chem. Soc.* **2016**, *138*, 2319–2326.

(25)	Menagen, G.; Macdonald, J. E.; Shemesh, Y.; Popov, I.; Banin, U. Au Growth on Semiconductor Nanorods: Photoinduced *versus* Thermal Growth Mechanisms. *J. Am. Chem. Soc.* **2009**, *131*, 17406–17411.

(26)	Wuister, S. F.; De Mello Donegá, C.; Meijerink, A. Luminescence Temperature Antiquenching of Water-Soluble CdTe Quantum Dots: Role of the Solvent. *J. Am. Chem. Soc.* **2004**, *126*, 10397–10402.

(27)	Zenkevich, E.; Stupak, A.; Göhler, C.; Krasselt, C.; von Borczyskowski, C. Tuning Electronic States of a CdSe/ZnS Quantum Dot by Only One Functional Dye Molecule. *ACS Nano* **2015**, *9*, 2886–2903.

(28)	Yang, S.; Prendergast, D.; Neaton, J. B. Tuning Semiconductor Band Edge Energies for Solar Photocatalysis *via* Surface Ligand Passivation. *Nano Lett.* **2012**, *12*, 383–388.

(29)	Brown, P. R.; Kim, D.; Lunt, R. R.; Zhao, N.; Bawendi, M. G.; Grossman, J. C.; Bulović, V. Energy Level Modification in Lead Sulfide Quantum Dot Thin Films through Ligand Exchange. *ACS Nano* **2014**, *8*, 5863–5872.

(30)	Carbone, L.; Nobile, C.; De Giorgi, M.; Sala, F. Della; Morello, G.; Pompa, P.; Hytch, M.; Snoeck, E.; Fiore, A.; Franchini, I. R.; Nadasan, M.; Silvestre, A. F.; Chiodo, L.; Kudera, S.; Cingolani, R.; Krahne, R.; Manna, L. Synthesis and Micrometer-Scale Assembly of Colloidal CdSe/CdS Nanorods Prepared by a Seeded Growth Approach. *Nano Lett.* **2007**, *7*, 2942–2950.

(31)	Gomes, R.; Hassinen, A.; Szczygiel, A.; Zhao, Q.; Vantomme, A.; Martins, J. C.; Hens, Z. Binding of Phosphonic Acids to CdSe Quantum Dots: A Solution NMR Study. *J. Phys. Chem. Lett.* **2011**, *2*, 145–152.

(32)	Chen, O.; Zhao, J.; Chauhan, V. P.; Cui, J.; Wong, C.; Harris, D. K.; Wei, H.; Han, H.-S.; Fukumura, D.; Jain, R. K.; Bawendi, M.G. Compact High-Quality CdSe–CdS Core–Shell Nanocrystals with Narrow Emission Linewidths and Suppressed Blinking. *Nat. Mater.* **2013**, *12*, 445–451.

(33)	Hanifi, D. A.; Bronstein, N. D.; Koscher, B. A.; Nett, Z.; Swabeck, J. K.; Takano, K.; Schwartzberg, A. M.; Maserati, L.; Vandewal, K.; van de Burgt, Y.; Salleo, A.; Alivisatos, A. P. Redefining Near-Unity Luminescence in Quantum Dots with Photothermal Threshold Quantum Yield. *Science* **2019**, *363*, 1199–1202.

(34)	Hens, Z.; Martins, J. C. A Solution NMR Toolbox for Characterizing the Surface Chemistry of Colloidal Nanocrystals. *Chem. Mater.* **2013**, *25*, 1211–1221.

(35) Ding, T. X.; Olshansky, J. H.; Leone, S. R.; Alivisatos, A. P. Efficiency of Hole Transfer from Photoexcited Quantum Dots to Covalently Linked Molecular Species. *J. Am. Chem. Soc.* **2015**, *137*, 2021–2029.

(36) Knauf, R. R.; Lennox, J. C.; Dempsey, J. L. Quantifying Ligand Exchange Reactions at CdSe Nanocrystal Surfaces. *Chem. Mater.* **2016**, *28*, 4762–4770.

(37) Hassinen, A.; Moreels, I.; De Nolf, K.; Smet, P. F.; Martins, J. C.; Hens, Z. Short-Chain Alcohols Strip X-Type Ligands and Quench the Luminescence of PbSe and CdSe Quantum Dots, Acetonitrile Does Not. *J. Am. Chem. Soc.* **2012**, *134*, 20705–20712.

(38) Balan, A. D.; Eshet, H.; Olshansky, J. H.; Lee, Y. V.; Rabani, E.; Alivisatos, A. P. Effect of Thermal Fluctuations on the Radiative Rate in Core/Shell Quantum Dots. *Nano Lett.* **2017**, *17*, 1629–1636.

(39) Rainò, G.; Stöferle, T.; Moreels, I.; Gomes, R.; Kamal, J. S.; Hens, Z.; Mahrt, R. F. Probing the Wave Function Delocalization in CdSe/CdS Dot-in-Rod Nanocrystals by Time-and Temperature-Resolved Spectroscopy. *ACS Nano* **2011**, *5*, 4031–4036.

(40) Snyder, R. G.; Strauss, H. L.; Elliger, C. A. C-H Stretchlng Modes and the Structure. 1. Long, Disordered Chains. *J. Phys. Chem.* **1982**, *86*, 5145–5150.

(41) Snyder, R. G.; Maroncelli, M.; Qi, S. P.; Strauss, H. L. Phase Transitions and Nonplanar Conformers in Crystalline N-Alkanes. *Science* **1981**, *214*, 188–190.

(42) Srinivasan, G.; Pursch, M.; Sander, L. C.; Müller, K. FTIR Studies of C 30 Self-Assembled Monolayers on Silica, Titania, and Zirconia. *Langmuir* **2004**, *20*, 1746–1752.

(43) Socrates, G. Alkane Group Residues: C-H Group. In *Infrared and Raman Characteristic Group Frequencies: Tables and Charts,* 3rd ed.; John Wiley & Sons: Chichester, 2001; pp 50–67.

(44) Schleeger, M.; Nagata, Y.; Bonn, M. Quantifying Surfactant Alkyl Chain Orientation and Conformational Order from Sum Frequency Generation Spectra of CH Modes at the Surfactant-Water Interface. *J. Phys. Chem. Lett.* **2014**, *5*, 3737–3741.

(45) Zhang, H.; Li, F.; Xiao, Q.; Lin, H. Conformation of Capping Ligands on Nanoplates: Facet-Edge-Induced Disorder and Self-Assembly-Related Ordering Revealed by Sum Frequency Generation Spectroscopy. *J. Phys. Chem. Lett.* **2015**, *6*, 2170–2176.

(46) Imry, Y. Finite-Size Rounding of a First-Order Phase Transition. *Phys. Rev. B* **1980**, *21*, 2042–2043.

(47) Challa, M. S. S.; Landau, D. P.; Binder, K. Finite-Size Effects at Temperature-Driven First-Order Transitions. *Phys. Rev. B* **1986**, *34*, 1841–1852.

(48) Luedtke, W. D.; Landman, U. Structure and Thermodynamics of Self-Assembled Monolayers on Gold Nanocrystallites. *J. Phys. Chem. B* **1998**, *102*, 6566–6572.

(49) Clayden, J.; Greeves, N.; Warren, S. Conformational Analysis. In *Organic*

Chemistry, 2nd ed.; Oxford University Press: Oxford, 2012; pp 360–381.

(50) Chen, Z.; Moore, J.; Radtke, G.; Sirringhaus, H.; O'Brien, S. Binary Nanoparticle Superlattices in the Semiconductor−Semiconductor System: CdTe and CdSe. *J. Am. Chem. Soc.* **2007**, *129*, 15702–15709.

(51) Salem, L. Attractive Forces between Long Saturated Chains at Short Distances. *J. Chem. Phys.* **1962**, *37*, 2100–2113.

(52) Voznyy, O. Mobile Surface Traps in CdSe Nanocrystals with Carboxylic Acid Ligands. *J. Phys. Chem. C* **2011**, *115*, 15927–15932.

(53) Kroupa, D. M.; Vörös, M.; Brawand, N. P.; McNichols, B. W.; Miller, E. M.; Gu, J.; Nozik, A. J.; Sellinger, A.; Galli, G.; Beard, M. C. Tuning Colloidal Quantum Dot Band Edge Positions through Solution-Phase Surface Chemistry Modification. *Nat. Commun.* **2017**, *8*, 15257.

(54) Liu, J.; Kilina, S. V.; Tretiak, S.; Prezhdo, O. V. Ligands Slow Down Pure-Dephasing in Semiconductor Quantum Dots. *ACS Nano* **2015**, *9*, 9106–9116.

(55) Frederick, M. T.; Achtyl, J. L.; Knowles, K. E.; Weiss, E. A.; Geiger, F. M. Surface-Amplified Ligand Disorder in CdSe Quantum Dots Determined by Electron and Coherent Vibrational Spectroscopies. *J. Am. Chem. Soc.* **2011**, *133*, 7476–7481.

(56) Bronstein, N. D.; Martinez, M. S.; Kroupa, D. M.; Vörös, M.; Lu, H.; Brawand, N. P.; Nozik, A. J.; Sellinger, A.; Galli, G.; Beard, M. C. Designing Janus Ligand Shells on PbS Quantum Dots Using Ligand–Ligand Cooperativity. *ACS Nano* **2019**, *13*, 3839–3846.

(57) Jasieniak, J.; Smith, L.; Embden, J. van; Mulvaney, P.; Califano, M. Re-Examination of the Size-Dependent Absorption Properties of CdSe Quantum Dots. *J. Phys. Chem. C* **2009**, *113*, 19468–19474.

(58) Bronstein, N. D.; Yao, Y.; Xu, L.; O'Brien, E.; Powers, A. S.; Ferry, V. E.; Alivisatos, A. P.; Nuzzo, R. G. Quantum Dot Luminescent Concentrator Cavity Exhibiting 30-Fold Concentration. *ACS Photonics* **2015**, *2*, 1576–1583.

TOC Graphic: